Commensurate and incommensurate magnetic structure of UNiGe

Nakotte, H.; Purwanto, A.; Robinson, R.A.; Tun, Z.; Prokes, K.; Larson, A.C.; Havela, L.; Sechovsky, V.; Maletta, H.; Bruck, E.H.; de Boer, F.R.

Published in:
Physical Review. B, Condensed Matter

DOI:
10.1103/PhysRevB.54.7201

Commensurate and incommensurate magnetic structures of UNiGe

H. Nakotte
Los Alamos National Laboratory, Los Alamos, New Mexico 87545

A. Purwanto*
Los Alamos National Laboratory, Los Alamos, New Mexico 87545
and Physics Department, New Mexico State University, Las Cruces, New Mexico 88003

R. A. Robinson
Los Alamos National Laboratory, Los Alamos, New Mexico 87545

Z. Tun
Chalk River Laboratories, Atomic Energy of Canada Limited, Chalk River, Ontario, Canada, K0J 1J0

K. Prokeš
Van der Waals-Zeeman Institute, University of Amsterdam, Valckenierstraat 65, 1018 XE Amsterdam, The Netherlands

Allen C. Larson
Los Alamos National Laboratory, Los Alamos, New Mexico 87545

L. Havela and V. Sechovský
Department of Metal Physics, Charles University, 12116 Prague 2, The Czech Republic

H. Maletta
Hahn-Meitner Institute, 14109 Berlin, Germany

E. Brück and F. R. de Boer
Van der Waals-Zeeman Institute, University of Amsterdam, Valckenierstraat 65, 1018 XE Amsterdam, The Netherlands
(Received 22 January 1996; revised manuscript received 24 April 1996)

A single crystal of the orthorhombic intermetallic compound UNiGe has been studied at both steady-state and pulsed neutron sources in its commensurate ($T<41.5$ K) and incommensurate ($41.5<T<51$ K) magnetic phases. The ordering wave vector in both phases is $\mathbf{q}=(0,\delta,\delta)$, with $\delta=1/2$ in the commensurate phase. δ is temperature dependent in the incommensurate phase, increasing from 0.35 at 50 K to 0.37 at 44 K. Irreducible representation theory is used to discuss the possible moment configurations in real space, and least-squares refinement gives a moment of $0.36\mu_B$ at 46 K, compared with $0.96\mu_B$ at 20 K. While symmetry allows moment components along all three Cartesian directions, previous unpolarized-neutron-diffraction data had been analyzed in terms of a collinear arrangement of moments in the b-c plane. Polarized neutron diffraction in the low-temperature commensurate phase shows that it is noncollinear, with an additional x component to the uranium moment, and there is some evidence that this is also the case in the incommensurate phase. The polarized-neutron measurement gives a canting angle, with respect to the b-c plane, of $17\pm4°$. The observed μ_x components are discussed in terms of bonding of the $5f$-electron orbitals with the surrounding ligands. [S0163-1829(96)00934-4]

I. INTRODUCTION

Uranium intermetallic compounds with the orthorhombic TiNiSi (space group $Pnma$) structure have been studied for a number of years.[1–3] In this structure, the uranium ions form chains along the a axis, albeit with small alternating displacements in the z direction, as shown in Fig. 1. In general, both neutron-diffraction and high-field magnetization studies indicate that the orthorhombic a axis is the hard magnetization axis and that the uranium moments lie in the orthorhombic b-c plane in a wide range of such UTGe compounds[4] (T=transition metal). The magnetic anisotropy is consistent with a more general phenomenology,[4] namely that the uranium moments in hybridizing intermetallic compounds lie systematically perpendicular the nearest-neighbor U-U links. This idea has some physical rationale, as an extension of theoretical work on cubic Ce compounds by Cooper *et al.*[5] Cooper's result is that the cerium $4f$-electron hybridizes with the ligand p electrons resulting in anisotropic exchange between neighboring cerium sites. The exchange between nearest cerium (or uranium) neighbors is ferromagnetic and the anisotropy is such that moments prefer to lie perpendicular to these strongly hybridized Ce-Ce (or U-U) links. However, the TiNiSi structure-type uranium intermetallic compounds are different from the Ce compounds discussed by Cooper *et al.* in several important respects: first, we are deal-

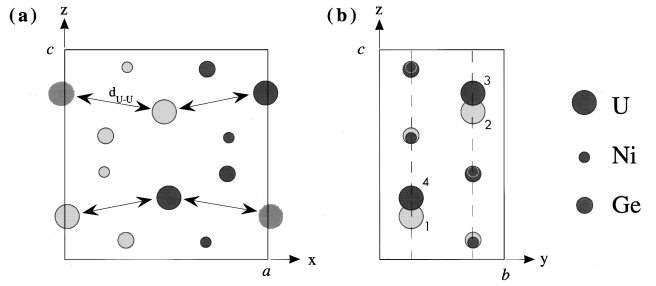

FIG. 1. The crystallographic structure of UNiGe shown as projections (a) onto the a-c and (b) onto the b-c planes. All unit-cell dimensions (represented by solid rectangles) and atomic positions are drawn to scale. In (a), the nearest U-U distance $d_{U\text{-}U}$ is shown by doubled-headed arrows. Note the slight zig-zag of $d_{U\text{-}U}$. In (b), the two mirror planes perpendicular to the b axis are shown as dashed lines: all atoms lie in these planes at $y=\pm 1/4$. Also in (b), the atoms represented by light colors lie below those represented by dark colors. The labeling of uranium atoms (1–4) corresponds to that given in Table I. The reader is referred to Ref. 10 for a complete list of structural parameters.

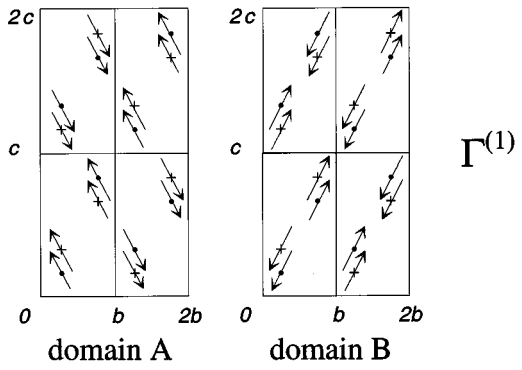

FIG. 2. The two possible magnetic domains belonging to the $\Gamma^{(1)}$ irreducible representation, derived for the low-temperature magnetic structure of UNiGe in Ref. 10. For the sake of clarity only the U atoms are drawn. The dimensions and positions are not drawn to scale. The arrows represent the moment components in the b-c plane. The dots and crosses represent the symmetry-allowed μ_x moment components parallel and antiparallel to the a axis, respectively.

ing with orthorhombic (rather than cubic) compounds with more pronounced intrinsic crystalline anisotropy; secondly while Ce has the possibility of one $4f$ electron, uranium has two or three $5f$ electrons, depending on its valence; and finally, Cooper discussed only compounds containing p-electron elements, while we are studying ternaries with additional transition-metal constituents and the hybridization between f and d electrons is likely to be more important. Nevertheless, Cooper's picture works remarkably well for a large number of uranium intermetallics.

In the particular case of UNiGe, there was originally thought to be one magnetic transition from paramagnetism to antiferromagnetism at 41.5 K, and the low-temperature magnetic structure was thought to be collinear with moments either along **b** (Ref. 6) or **c**.[3] However, subsequent specific-heat[7,8] and magnetization[9] measurements have shown the presence of two magnetic phase transitions at 41.5 and 51 K, respectively. Furthermore, neutron-diffraction studies on a single crystal have shown that the moments in the low-temperature commensurate phase are not purely parallel to **b** or **c**,[10] and that the magnetic structure is as shown in Fig. 2. It is a single-**q** magnetic structure with $\mathbf{q}=(0,1/2,1/2)$, and belongs to one of two possible irreducible representations, as discussed in Ref. 10. Both domains of this structure (see Fig. 2) were observed, and symmetry allows moment components along all three Cartesian axes. Between 41.5 and 51 K UNiGe is incommensurate[9,10] with $\mathbf{q}=(0,\delta,\delta)$, but the detailed geometrical arrangement of the moments has not been discussed previously. The essential features of the B-T phase diagram[10,11] are shown in Fig. 3, and we note that a further $\mathbf{q}=(0,1/3,1/3)$ commensurate phase can be induced in applied magnetic fields.[8]

In our previous paper[10] on the zero-field commensurate antiferromagnetic structure of UNiGe, we used irreducible representation theory to sort through the possible moment configurations. Of the two possible irreducible representations $\Gamma^{(1)}$ and $\Gamma^{(2)}$, the former was clearly in better agreement with the data. The in-plane (in b-c plane) moment components are ferromagnetically coupled for U moments in the same a-axis chain. These in-plane components are collinear and point in a direction somewhat aligned towards $\mathbf{q}=(0,1/2,1/2)$. However, symmetry also allows moment components along the x axis and the refinement actually preferred such additional nonzero μ_x contributions, with the moments canted out of the b-c plane by 20° or so. The resultant configuration is noncollinear, and is shown in Fig. 2. Even though such μ_x components are allowed by symmetry, we were reluctant to give too much credence to them, as their presence could only be inferred from a number of relatively weak reflections which would also be present if $\mu_x=0$. The first part of this article covers a polarized-neutron study of the low-temperature commensurate phase, on the same crystal. We show definitively that such noncollinear μ_x components are indeed present, a conclusion that is at odds with the simple relationship between magnetic anisotropy and hybridization described above. The purpose of the second part of

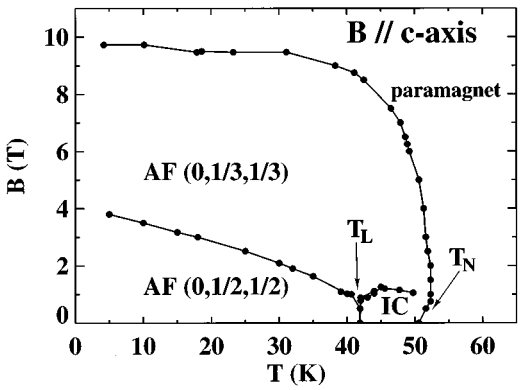

FIG. 3. The **B**-T magnetic phase diagram for magnetic field **B** parallel to the b axis, as determined by high-field magnetization. The phase diagram for **B** parallel to **b** is topologically similar, but with higher transition fields, while that for **B** parallel to **c**, shows no transitions up to 35 T. T_N and T_L denote the zero-field Néel and lock-in transition temperatures at 41.5 and 51 K, respectively. In applied magnetic fields, a third magnetically ordered phase with $\mathbf{q}=(0,1/3,1/3)$ occurs (Ref. 8).

the article is to characterize the zero-field incommensurate magnetic phase between 41.5 and 51 K and to discuss its relationship to the low-temperature commensurate phase.

II. METHODS

The $2\times2\times1.6$ mm^3 single crystal of UNiGe was grown by a modified Czochralski tri-arc technique and is the same one as used in the previous neutron measurements[10] and in the determination of the B-T magnetic phase diagram.[11] Four different diffractometers were used for the experiments: the single-crystal diffractometer (SCD) at the LANSCE spallation neutron source at Los Alamos, the N5 and C5 triple-axis spectrometers at the NRU reactor at Chalk River, and the E4 two-axis diffractometer at the Berlin Neutron Scattering Centre (BENSC). SCD is essentially a neutron Laue camera, in which the neutron wavelength is determined from its total time of flight between the pulsed source and the area detector. The SCD data were analyzed using the Generalized Structure Analysis System (GSAS),[12] with further analysis using purpose-written FORTRAN programs. In the triple-axis spectrometer N5, the analyzer was removed, and the intensities of relevant reflections were measured as rocking curves. The C5 triple-axis spectrometer was used for the polarized-neutron experiment described in the next section.

III. NONCOLLINEAR MAGNETIC ORDER IN UNiGe BELOW 41.5 K: IS THERE A μ_x COMPONENT OR NOT?

The experiment to test for μ_x components to the uranium moment in the commensurate (0,1/2,1/2) phase was performed on the C5 polarized triple-axis spectrometer of the DUALSPEC facility at Chalk River Laboratories, Canada. We used the (111) Bragg reflection of Cu_2MnAl Heusler crystals to produce and analyze the polarized beams. The incident beam (collimated to about 0.8°) was filtered through a 10 cm sapphire filter cooled by liquid-N_2 and the wavelength selected by the monochromator was $\lambda=2.37$ Å. A graphite filter in the scattered beam was used to minimize $\lambda/2$ and $\lambda/3$ contamination. The polarization direction **P** of the neutrons at the sample position was the same as the guide field **B** (about 50 mT), generated by a horizontal-field cryomagnet. The magnet, designed specifically for neutron scattering, does not have pole pieces at the beam level. Consequently, it provides a large in-plane access (~350°) of neutron beams to the sample, with a small ''dark angle'' (~10°) caused by liquid-He transfer tubes. A Mezei flipper, arranged to rotate the neutron spin by π, was placed between the sample and the detector so that both spin-flip and non-spin-flip scattering from the sample could be measured. The crystal was mounted in the magnet with the b-c plane horizontal. In this configuration, the magnetic-field direction **B**, and therefore the polarization direction **P** of the neutrons, are in the b-c plane. A special drive mechanism allowed the sample to be rotated within the magnet. Since the magnet was mounted on a rotation table, by rotating the sample and the magnet by the same angle but in opposite directions, we could select **B** (and therefore **P**) to be in any direction within the b-c plane without changing the scattering vector **Q**. We can thus measure scattering response at different angles of the neutron polarization in the b-c plane.

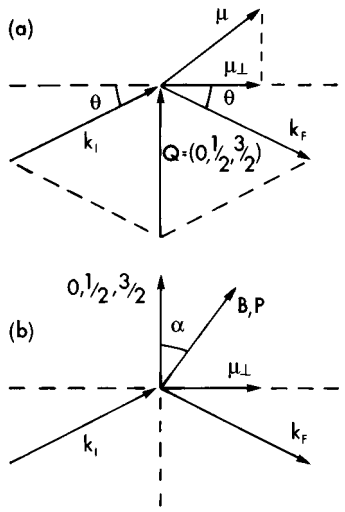

FIG. 4. Schematic scattering geometry for (a) unpolarized neutrons and (b) polarized neutrons, with an external field to determine the neutron polarization at the sample. **Q** is the scattering vector, $\boldsymbol{\mu}$ is the magnetic moment (which may have a μ_x component out of the plane of the paper), $\mu_\perp$ is its perpendicular component within the plane of the paper, and $\mathbf{k}_I$ and $\mathbf{k}_F$ denote the incident and final scattering wave vectors, respectively. In (b) the polarization direction of the neutrons is defined by a magnetic-field direction denoted by **B**, and α gives the angle between **B** and **Q**. All physically relevant vectors lie in the plane of the paper (i.e., the b-c plane), except for the μ_x component to the uranium moment which points into or out of the plane of the paper.

In any type of magnetic neutron scattering, polarized or unpolarized, one is only sensitive to those components of the magnetic moment which are perpendicular to the wave-vector transfer **Q**. As shown in Fig. 4(a), this means that for **Q**=(0,1/2,3/2), magnetic scattering arises only from the $\mu_\perp$ (the component of μ which lies in the b-c plane and is perpendicular to **Q**) and μ_x components to the magnetic moment. If one uses polarized neutrons, the polarization direction **P** is defined by the magnetic field **B** as shown in Fig. 4(b). Therefore, we can define an angle α between **B** (or the polarization **P**) and the scattering vector **Q**. In a polarized-neutron experiment, the magnetic scattering is divided into spin-flip and non-spin-flip scattering, I_{SF} and I_{NSF}. The spin-flip channel sees only components of the moment perpendicular to **P**, while the non-spin-flip channel sees only the parallel components. This means that if the moments in the sample are arranged in a collinear arrangement within the b-c plane (i.e., $\mu_x=0$), magnetic intensity can arise only from that in-plane component of the magnetic moment which is also perpendicular to **Q**, i.e., $\mu_\perp$ in Fig. 4. There will be no contribution to spin-flip scattering, i.e., $I_{\mathrm{SF}}=0$, for **B** (or **P**) perpendicular to **Q**, and we expect to find the angular dependences for spin-flip and non-spin-flip scattering shown in Fig. 5(a). If, however, there is a nonzero μ_x contribution to the magnetic moment then $I_{\mathrm{SF}}\neq0$, and we should find angular dependences as shown in Fig. 5(b).

A full evaluation of the cross sections of spin-flip and non-spin-flip scattering is given in Ref. 13. We summarize here only the results needed for the present case:

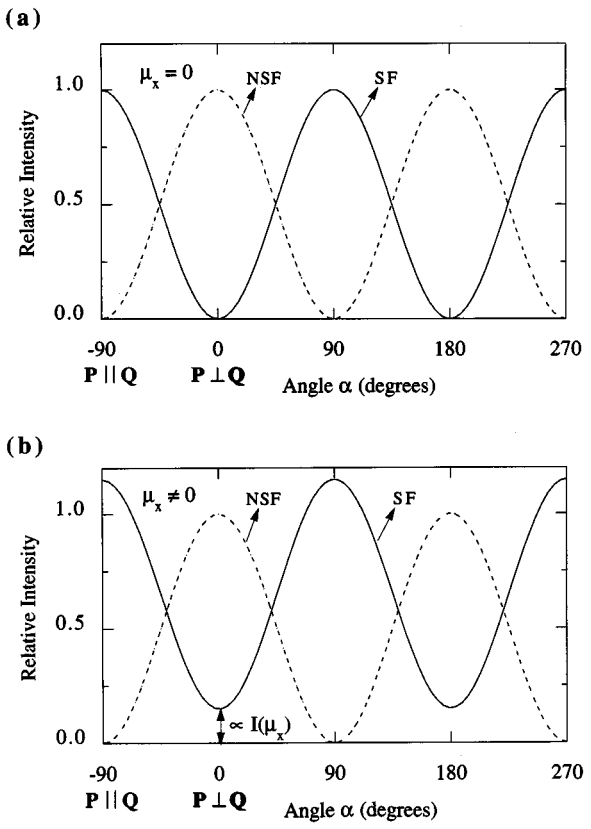

FIG. 5. Idealized behavior for the variation of the spin-flip (SF) and non-spin-flip (NSF) cross sections for the (0,1/2,3/2) magnetic reflection as a function of magnetic-field angle α, (a) assuming $\mu_x = 0$ and (b) assuming that $\mu_x \neq 0$. Note that the minimum in the spin-flip curve is no longer equal to the minimum in the non-spin-flip curve, and that the difference between the minima is proportional to $(\mu_x)^2$.

$$\begin{aligned} \mathbf{P}\|\mathbf{Q}\text{:}\quad & \text{spin-flip scattering} \quad I_{\mathrm{SF}} \propto (\mu_\perp)^2 + (\mu_x)^2, \\ & \text{non-spin-flip scattering} \quad I_{\mathrm{NSF}} = 0, \\ \mathbf{P}\perp\mathbf{Q}\text{:}\quad & \text{spin-flip scattering} \quad I_{\mathrm{SF}} \propto (\mu_x)^2, \\ & \text{non-spin-flip scattering} \quad I_{\mathrm{NSF}} \propto (\mu_\perp)^2. \end{aligned} \tag{1}$$

The reader is reminded that, in our notation, $\mu_\perp$ denotes the component of μ which lies in the b-c plane and is perpendicular to **Q**. Equation (1) demonstrates that any difference between the non-spin-flip scattering for **P** parallel to **Q** and spin-flip scattering for **P** perpendicular to **Q** is a direct measure of the existence of a μ_x component in the magnetic moment. Note, however, that the present configuration does not provide any information on the direction of moment components within the b-c plane.

For the experiment, we chose the (0,1/2,3/2) magnetic reflection as its calculated magnetic structure factor is relatively large and it is particularly sensitive to the presence of μ_x. There is no contamination from the misaligned crystallites reported in Ref. 10. This is because the (0,1,0) reflection of the crystallite, which would contribute on the (0,1/2,3/2) position of the parent phase, is systematically absent. The integrated intensities of spin-flip and non-spin-flip contributions to the (0,1/2,3/2) magnetic reflection were measured as a function of α in 5° steps and are shown in Fig. 6. The scale was calibrated in such way that for $\alpha = 0°$, the applied field was roughly parallel to **Q**. At each position, we also measured the integrated intensity of the (0,0,4) nuclear reflection, which is purely non-spin flip in character. The measurement of a nuclear reflection allows correction for various effects. Firstly, there is a small spurious contribution to the spinflip scattering due to the fact that the overall polarization efficiency is only 96% rather than 100%. Secondly, depolarization effects may also lead to increased intensity in the spin-flip channel (non-negligible depolarization effects were found only in a rather small angular range of about 10°, well removed from that used for the main measurement). The most significant corrections (up to 12% in the intensities), however, were found to be due to differences in absorption of the cryostat and/or slight misalignment of the sample. This was reflected in changes in the sum of the integrated intensities of spin-flip and non-spin-flip scattering ($I_{\mathrm{SF}} + I_{\mathrm{NSF}}$) as a function of α. Corrections for these effects were made in the analysis of intensities given below.

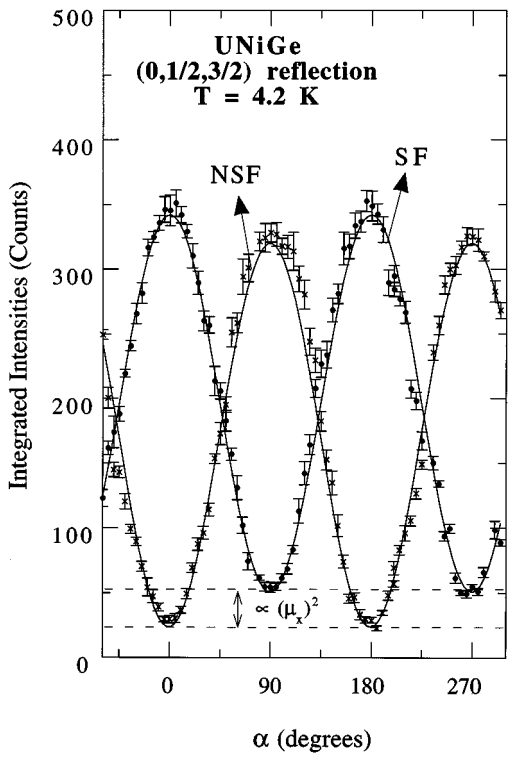

FIG. 6. Integrated intensities of spin-flip (SF) and non-spin-flip (NSF) contributions to the magnetic (0,1/2,3/2) reflection as a function of α, the angle between the neutron polarization **P** and the scattering vector **Q** [see Fig. 4(b)]. Note that there is a clear difference between the minimum responses for the spin-flip and non-spin-flip scattering, which is due to the μ_x contribution to the $5f$ moment of UNiGe. The solid lines represent the fits to the sinusoidal function described in the text.

Figure 6 shows the integrated spin-flip and non-spin-flip contributions to the magnetic scattering in UNiGe as a function of the angle α. As expected, the minima in the response for spin-flip and non-spin-flip scattering are found around 90° (**P**⊥**Q**) and 0° (**P**∥**Q**), respectively. There is also a clear

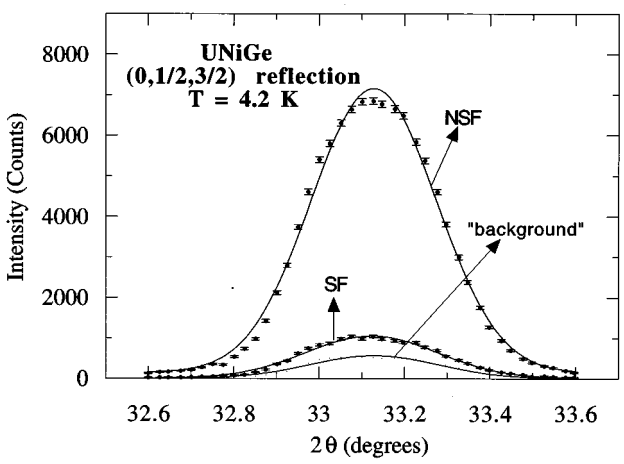

FIG. 7. 2θ scans of the spin-flip (SF) and non-spin-flip (NSF) contributions to the magnetic (0,1/2,3/2) reflection for $\mathbf{P}\perp\mathbf{Q}$ (i.e., $\alpha=90°$). In the plot, we have also displayed the ''background'' (i.e., the non-spin-flip scattering at $\alpha=0°$). The solid lines are fits to Gaussian distributions.

difference between the integrated intensities of spin-flip and non-spin-flip scattering at the minimum positions. This difference is incontrovertible evidence for a nonzero μ_x. The data were fitted using the function $I(\alpha)=A+B\sin^2(\alpha+\phi)$. The spin-flip and non-spin-flip intensities were constrained to be 90° out of phase with each other, but all other parameters were allowed to vary. The resulting fits are denoted in Fig. 6 by solid lines.

In order to obtain a quantitative estimate for the out-of-plane canting, we also measured the 2θ scans for spin-flip and non-spin-flip scattering at $\alpha=90°$, where $\mathbf{P}\perp\mathbf{Q}$. To achieve sufficient statistics each point was counted for more than 20 min. We also measured the integrated intensity arising in non-spin-flip scattering at $\alpha=0°$ (where $\mathbf{P}\|\mathbf{Q}$), which gives a measure of the nonmagnetic ''background.'' The raw data are shown in Fig. 7. Apart from real background (which should be flat) there is a 4% spin-flip contribution in the ''background'' signal (due to ''leakage'' in the overall polarization), but most of the ''background'' is likely due to imperfect positioning of the minimum and/or some small remaining $\lambda/2$ contamination due to the (0,1,3) nuclear reflection. After correction for these effects, the intrinsic intensities for spin-flip and non-spin-flip scattering, I_{SF} and I_{NSF}, were extracted. These quantities are related to the total moment μ and its x component μ_x by the following expression:

$$\frac{\mu_x}{\mu}=\cos\theta=\left(\frac{I_{\mathrm{SF}}^{\alpha=90}}{I_{\mathrm{NSF}}^{\alpha=90}}\right)^{1/2}, \tag{2}$$

where $90-\theta$ is the canting angle out of the b-c plane. Our analysis yields an out-of-plane canting angle of $17\pm4°$. This is in reasonable agreement with the value obtained by least-squares refinement in Ref. 10, which gave an out-of-plane angle of $21.3\pm0.8°$.

This analysis assumes that the moment lies solely on the uranium sublattice, with no hybridization-induced moment on the Ni. If, on the other hand, the difference between the minima in I_{SF} and I_{NSF}, were to be attributed to Ni moments, the same reasoning would apply. Any such Ni moment would have to possess substantial moment components perpendicular to those of the uranium sublattice. This is somewhat implausible for induced moments, and we therefore believe our interpretation is basically correct, even if there are extra small moments on the Ni sublattice.

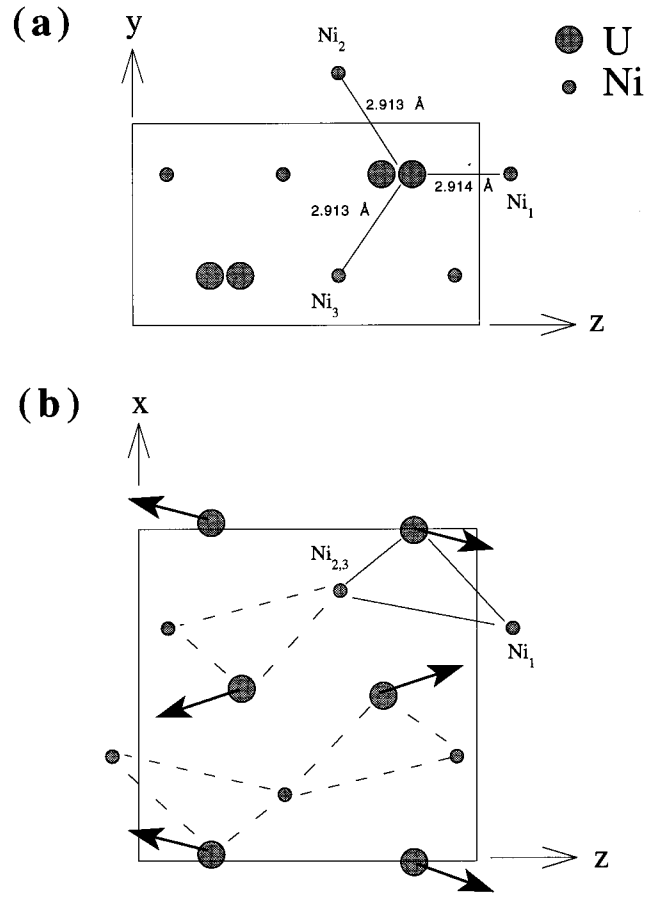

FIG. 8. The locations of the U and Ni atoms in UNiGe shown as a projections (a) onto the b-c and (b) onto the a-c plane. All dimensions are drawn to scale. The unit cells are indicated by the solid rectangles. Note that each U atom has three closest Ni neighbors (Ni_1, Ni_2, and Ni_3). The three shortest U-Ni links for a particular U atom are represented by solid lines, and the corresponding distances are given in (a). In (b), the shortest U-Ni links for the other U atoms are shown by dashed lines. Also in (b), the stacking of magnetic moments in one crystallographic cell is indicated by arrows. Note, however, that the moment stacking is different in the adjacent crystallographic cells (see text).

To summarize, the main result of this section is the definitive evidence for a significant nonzero μ_x contribution to the uranium moment in the low-temperature commensurate phase of UNiGe. The presence of this component makes the magnetic structure noncollinear, and different from the simple moment-density-wave-type structure discussed in Ref. 10. There are now two completely independent pieces of evidence that $\mu_x\neq0$: (1) the least-squares refinement[10] to the intensities of 40 independent magnetic reflections, as measured using unpolarized neutrons, which we were reluctant to believe, and (2) the present polarized-neutron experiment on the (0,1/2,3/2) magnetic reflection, in which the dependence of the spin-flip and non-spin-flip cross sections on neutron-polarization direction (with respect to $\mathbf{Q}$) was exploited.

This result is important in that it clearly contradicts the simple physical picture given in the introduction. This picture would imply that any uranium moments would lie in the b-c plane and have no x component. Even though the uranium chains have a slight zig-zag, with displacements in the z direction (with an angle of 10° or so), each uranium atom has two equally distant nearest-neighbor uranium atoms (see Fig. 1). Therefore, symmetry would still dictate that $\mu_x = 0$, so long as the important interaction is between uranium ions. The essence of Cooper's picture[5] is of anisotropic exchange between uranium ions, albeit mediated by hybridization (including many-body correlation effects) between the uranium f electrons and the ligand p and d electrons. The vast majority of uranium intermetallic compounds studied so far seem to comply with the rule that the moments systematically lie perpendicular to U-U nearest-neighbor links. UNiGe therefore seems to be somewhat anomalous.

While all the atoms in the TiNiSi structure type lie in mirror planes at $y = \pm 1/4$, there are no mirror planes perpendicular to the x-axis uranium chains (see Fig. 1). Viewed from any one of the uranium ions, this lack of symmetry manifests itself in two ways: first, there are two chains per unit cell, and these chains are displaced (along x) with respect to each other; second, and more importantly, the distribution of Ni and Ge ions around each uranium site is highly asymmetric. The uranium point-group only contains the mirror plane in the x-z plane, and it turns out that each uranium ion has three nearest-neighbor Ni ions as shown in Fig. 8. If interactions between Ni ions and U moments are important in determining the anisotropy, the asymmetry in f-d hybridization may give a mechanism for the canting out of the b-c plane. As shown in Fig. 8(b), it is very suggestive that the projected moment directions are almost parallel to the plane containing the three nearest-neighbor Ni atoms. However, any argument that works for an individual chain, in Fig. 8(b), breaks down if we propagate it to the adjacent crystallographic cells shown in Fig. 2, as is required by the antiferromagnetic structure. Nevertheless, the present experiment provides clear evidence the direct f-d interactions may be important, and it would be very helpful if theoretical work could be performed to clarify this point. Two approaches have been used to date for this type of problem. First there is the regular total-energy electronic band-structure, but including relativistic spin-orbit coupling and allowing noncollinearity, as performed by Sandratskii and Kübler[14] for U_2Pd_2Sn and U_3P_4. The second approach due to Cooper[5] and co-workers includes the many-body contribution to the hybridization explicitly, but is based on a simpler band-structure calculation.

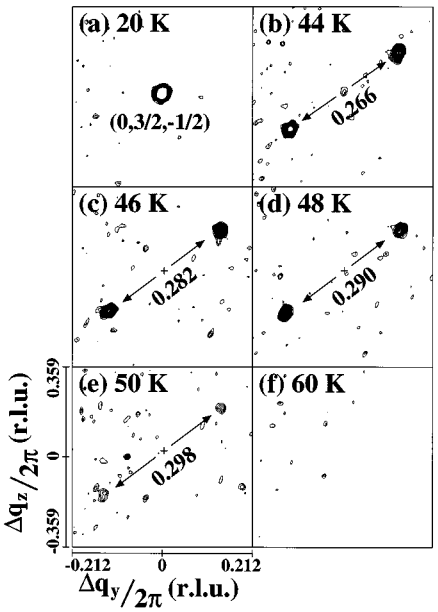

FIG. 9. The temperature evolution of magnetic intensity in the vicinity of the $(0,3/2,-1/2)$ point, as measured on SCD at Los Alamos. The commensurate $(0,3/2,-1/2)$ antiferromagnetic reflection splits into two $(0,\delta,\delta)$-type satellites above 41.5 K and their intensities decrease continuously before they disappear at 51 K.

IV. INCOMMENSURATE MAGNETIC STRUCTURE OF UNiGe BETWEEN 41.5 AND 51 K.

Portions of the raw unpolarized neutron data taken on SCD in the vicinity of the $(0,3/2,-1/2)$ point are shown in Fig. 9. The commensurate (0,3/2,1/2) reflection splits into

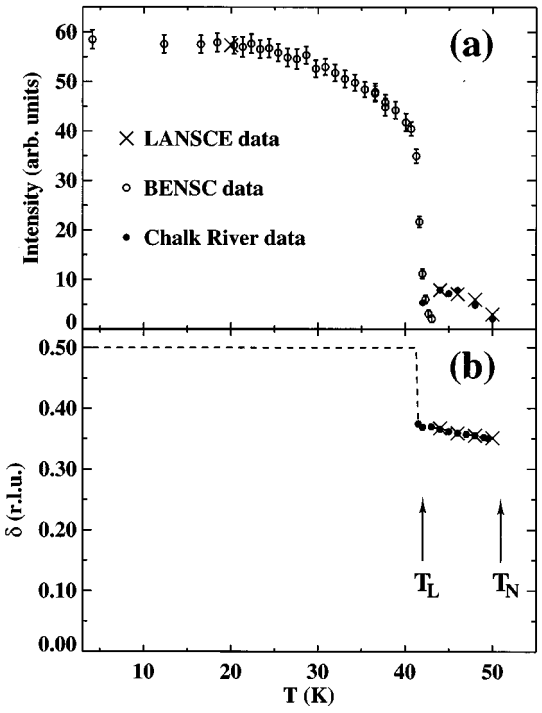

FIG. 10. The temperature dependences of (a) the magnetic diffraction intensity and (b) the magnetic propagation vector δ, in both the commensurate antiferromagnetic phase ($T < 41.5$ K) and the incommensurate phase ($41.5 < T < 51$ K). For the incommensurate phase, the sum over both satellites was used. The intensities were corrected for the variations in both the U^{3+} form factor and the Lorentz factor. The crosses represent data taken at LANSCE, while the open circles represent data taken in the commensurate phase at BENSC and the solid circles represent data taken in the incommensurate phase at Chalk River. The $(0,3/2,-1/2)$ reflection and its associated satellites were used in this analysis. The new results for the temperature dependence of δ given in (b) are in very good agreement with independent measurements previously reported in Ref. 9.

TABLE I. Possible moment phase relations for the incommensurate phase of UNiGe with $\mathbf{q}=(0,\delta,\delta)$.

Phase relation	Atom[a]	Representation $\check{\Gamma}^{(1)}$			Representation $\check{\Gamma}^{(2)}$		
		μ_x	μ_y	μ_z	μ_x	μ_y	μ_z
i	1 $(x,1/4,z)$	+	+	+	+	+	+
	2 $(1/2-x,3/4,1/2+z)$	+	−	−	−	+	+
	3 $(-x,3/4,-z)$	+	−	−	−	+	+
	4 $(1/2+x,1/4,1/2-z)$	+	+	+	+	+	+
ii	1	+	+	+	+	+	+
	2	+	−	−	−	+	+
	3	−	−	−	+	+	+
	4	−	+	+	−	+	+
iii	1	+	+	+	+	+	+
	2	+	−	−	−	+	+
	3	+	+	−	−	+	+
	4	+	−	+	+	−	+
iv	1	+	+	+	+	+	+
	2	+	−	−	−	+	+
	3	+	−	+	−	+	−
	4	+	+	−	+	+	−
v	1	+	+	+	+	+	+
	2	+	−	−	−	+	+
	3	+	+	+	−	−	−
	4	+	−	−	+	−	−
vi	1	+	+	+	+	+	+
	2	+	−	−	−	+	+
	3	−	−	+	+	+	−
	4	−	+	−	−	+	−
vii	1	+	+	+	+	+	+
	2	+	−	−	−	+	+
	3	−	+	−	+	−	+
	4	−	−	+	−	−	+
viii	1	+	+	+	+	+	+
	2	+	−	−	−	+	+
	3	−	+	+	+	−	−
	4	−	−	−	−	−	−

[a] $x=0.0111$, $z=0.2054$, from Ref. 10.

TABLE II. Reduced χ^2 and moment amplitudes for the models listed in Table I.

Phase relation	Representation $\check{\Gamma}^{(1)}$		Representation $\check{\Gamma}^{(2)}$	
	U moment (μ_B)	Reduced χ^2	U moment (μ_B)	Reduced χ^2
i	0.26±0.02	2.20	0.31±0.01	2.31
ii	0.36±0.03	2.09	0.33±0.02	3.08
iii	0.35±0.02	2.28	0.42±0.04	2.19
iv	0.39±0.04	2.51	0.38±0.03	2.31
v	0.50±0.03	2.54	0.43±0.03	2.13
vi	0.37±0.02	2.46	0.39±0.03	3.13
vii	0.39±0.01	2.16	0.44±0.04	3.05
viii	0.41±0.04	3.19	0.47±0.04	3.15
ii, in b-c plane	0.30±0.01	2.19		

TABLE III. Refined magnetic parameters for UNiGe at 46 K.

	$T=46$ K		$T=20$ K
	$\mu_x=0$	$\mu_x\neq 0$	(from Ref. 10)[a]
In spherical polar coordinates with $0<\theta<180°$ from a axis and $0<\phi<360°$ from b axis in b-c plane:			
μ (μ_B)	0.30±0.01	0.36±0.03	0.96±0.01
θ (degrees)	90.0 (fixed)	127±7	111.25±0.8
ϕ (degrees)	55±5	50±6	71.4±1.8
In Cartesian coordinates			
μ_x (μ_B) $=\mu\cos\theta$	0.00 (fixed)	−0.22±0.02	−0.35±0.01
μ_y (μ_B) $=\mu\sin\theta\cos\theta$	0.17±0.02	0.19±0.02	0.29±0.01
μ_z (μ_B) $=\mu\sin\theta\sin\phi$	0.24±0.02	0.23±0.02	0.85±0.01
Volume fraction in domain B (%)	66±3	67±5	61.1±0.7
Reduced χ^2	2.19	2.09	2.33

[a]Note that we report parameters according to the same convention for both phases, and for the majority domain, while Ref. 10 reported physically equivalent parameters for the minority domain.

two satellites, which separate further with increasing temperature until they disappear completely at the Néel temperature of 51 K. A total of 11 magnetic reflections were measured in this phase on SCD, and all could be indexed assuming a magnetic propagation vector of $[0,\delta,\delta]$. The temperature dependences of several of these magnetic reflections were studied further in Berlin and Chalk River. The full variation of the intensity of the $(0,3/2,-1/2)$ reflection, and the sum of the intensities in the corresponding incommensurate satellites, is shown in Fig. 10(a), while the variation of δ is shown in Fig. 10(b).

Irreducible-representation symmetry analysis[15] can be applied to the incommensurate phase, in much the same way as to the commensurate phase.[10] Again there are two possible representations $\breve{\Gamma}^{(1)}$ and $\breve{\Gamma}^{(2)}$, and both allow all three Cartesian moment components. However, while the moments on the four uranium sites in the crystallographic (nuclear) unit cell are related to each other by symmetry in the commensurate phase, they are only constrained pairwise in the incommensurate phase. Specifically, the moment on the (x,y,z) site is related to that on the $(1/2-x,1/2+y,1/2+z)$ site by a diagonal n glide with glide translation $(0,1/2,1/2)$. Likewise the moments on the other pair of atoms are related to each other, but symmetry does not constrain the phase relations of the pairs with respect to each other. As a consequence, the general model has up to nine independent parameters with which to describe the final magnetic structure: three Cartesian moment amplitudes for the first pair of uranium atoms, a further three for the other pair, and finally three independent phase factors to relate the first pair to the second. Given all these degrees of freedom, least-squares fitting to the observed intensities turns out to be a fairly ill-posed problem. We therefore limited our choice of possible models to those in which the moments on the x-axis chains are related by phase factors 0 and π for each Cartesian moment coordinate. Of course, these phase factors are superposed on the global $\exp(i\mathbf{q}\cdot\mathbf{r})$ phase. There are still eight possible models for $\breve{\Gamma}^{(1)}$ and eight for $\breve{\Gamma}^{(2)}$ and all 16 models are tabulated in Table I. The fitted total uranium moments and corresponding reduced χ^2 are listed in Table II. Irrespective of the model chosen, several robust features emerge. Firstly, the refinements all give a nonzero value for μ_x. Secondly, the moments range between 0.25 and $0.5\mu_B$. The best fit of these is $\breve{\Gamma}^{(1)}$ with choice (ii) for the moment configuration, though it is only marginally preferred over several other moment configurations. The fitted parameters for the $\breve{\Gamma}^{(1)}$ (ii) model, with and without $\mu_x=0$, are listed in Table III. If $\mu_x=0$, the system would conform to the type of

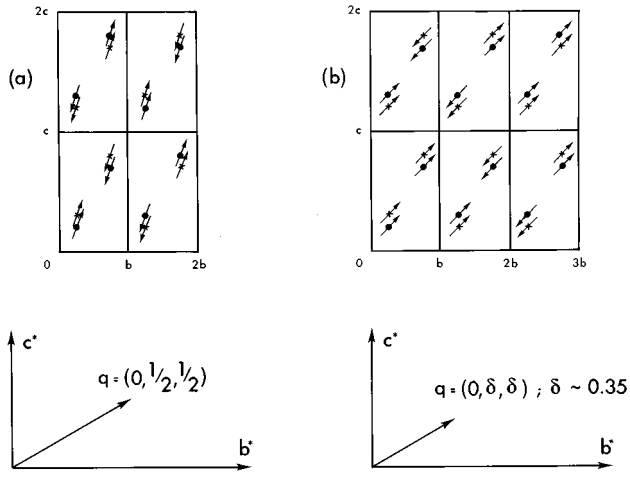

FIG. 11. The real-space moment configurations for one magnetic domain in UNiGe (a) in the commensurate antiferromagnetic phase below 41.5 K and (b) in the incommensurate phase between 41.5 and 51 K. Only uranium atoms are shown. The structures are represented as projections onto the b-c plane [as in Fig. 1(b)], four crystallographic unit cells being shown in (a) and six in (b). The in-plane components are shown by arrows, while the out-of-plane μ_x components are shown as crosses for moments tipping into the plane of paper and circles for those tipping out. All angles are drawn to scale, but the moment lengths are not. Note that the sequence of in-plane components on (011)-type planes in (a) is $+-+-$, while in (b) it is $++-++-$, but with a 180° phase shift (not shown) every twenty layers or so. The lower panels show the corresponding $\mathbf{q}$ vectors in reciprocal space. The relationship between the $\mathbf{q}=(0,0.35,0.35)$ incommensurate phase and the $\mathbf{q}=(0,1/3,1/3)$ phase shown in Fig. 3 is discussed in the text.

magnetic anisotropy discussed in the introduction, and the model would then essentially represent collinear in-plane moments with the moments at ~50° with respect to the *b* axis. The sequence on adjacent (011) planes of uranium atoms would tend more to a $++-$ arrangement, as opposed to the $+-+-$ sequence in the commensurate low-temperature phase. This $++-$ configuration is shown graphically in Fig. 11(b), but one should bear in mind that there is a π phase shift every 20 (011) layers or so.

The $++-$ arrangement immediately suggests a connection with the $\mathbf{q}=(0,1/3,1/3)$ commensurate phase seen in *c*-axis magnetic fields greater than 2 T (see Fig. 3). A strictly periodic $++-$ arrangement would have exactly $\mathbf{q}=(0,1/3,1/3)$, and would also have a net macroscopic moment. In other words it is likely to be induced by the application of an external field. So far, magnetisation experiments have been performed with fields parallel to the principal crystallographic axes **a**, **b**, and **c**. However the results reported here and in Ref. 10 indicate that the uranium moments prefer to align at an angle of 50° to 70° away from the *b* axis. It would clearly be fruitful to repeat both the magnetization measurements and the neutron-diffraction experiments with magnetic fields at other angles in the *b*-*c* plane. The transition field might well reach a minimum if applied parallel to the moment direction, and one might well be able to produce a monodomain sample.

Another important result is that, UNiGe probably possesses nonzero μ_x components in the incommensurate phase, just as in the low-temperature commensurate phase. These *x* components alternate up and own on the *a*-axis chains, just as in the low-temperature phase: both are shown in Fig. 11, and the configurations are very similar. While the in-plane components are parallel within a given *a*-axis chain, the *x* components alternate up and down. In other words, the incommensurate phase is simply related to the $\mathbf{q}=(0,1/2,1/2)$ commensurate phase. Taking this, together with the suggestive relationship to the field-induced $\mathbf{q}=(0,1/3,1/3)$ phase, we believe the $\check{\Gamma}^{(1)}$ (ii) model to be entirely plausible.

V. CONCLUSIONS

We have shown that the $\mathbf{q}=(0,\delta,\delta)$ incommensurate magnetic phase in UNiGe between 41.5 and 51 K is simply related to the $\mathbf{q}=(0,1/2,1/2)$ commensurate antiferromagnetic phase seen below 41.5 K. δ is slightly temperature-dependent with a value close to 0.35, which is in turn close to the propagation vector of the field induced phase seen above 2 T (with field parallel to **c**). In addition, we have given additional strong evidence that the low-temperature $\mathbf{q}=(0,1/2,1/2)$ magnetic structure is noncollinear, in that it has significant μ_x components to the uranium moment. There is also some evidence that there are similar μ_x components in the incommensurate phase.

ACKNOWLEDGMENTS

We are glad to acknowledge a number of very helpful discussions with Professor B. R. Cooper. This work was sponsored in part by the U.S. Czechoslovak Science and Technology Joint Fund in cooperation with the MSMT CR and the U.S. Department of Energy under Project No. 93039. It was also supported in part by the division of Basic Energy Sciences of the U.S. Department of Energy, by the Stichtung voor Fundamenteel Onderzoek der Materie (FOM), and by the Grant Agency of the Czech Republic (Project No. 202/94/0454).

*Permanent address, Materials Science Research Center, National Atomic Energy Agency, Serpong, Tangerang 15310, Indonesia.

[1] R. Troć and V. H. Tran, J. Magn. Magn. Mater. **73**, 389 (1988).

[2] V. Sechovský and L. Havela, in *Ferromagnetic Materials*, edited by E. P. Wohlfarth and K. H. J. Buschow (North-Holland, Amsterdam, 1988), Vol. IV, p. 309.

[3] S. Kawamata, K. Ishimoto, Y. Yamaguchi, and T. Komatsubara, J. Magn. Magn. Mater. **104–107**, 51 (1992).

[4] R. A. Robinson, A. C. Lawson, V. Sechovský, L. Havela, Y. Kergadallan, H. Nakotte, and F. R. de Boer, J. Alloys Compd. **213/214**, 528 (1994), and references therein.

[5] B. R. Cooper, R. Siemann, D. Yang, P. Thayamballi, and A. Banerjea, in *Handbook on the Physics and Chemistry of the Actinides*, edited by A. J. Freeman and G. H. Lander (North-Holland, Amsterdam, 1985), Vol. II, Chap. 6.

[6] A. Murasik, P. Fischer, R. Troć, and V. H. Tran, J. Phys. Condens. Matter **3**, 1841 (1991).

[7] K. Prokeš, H. Nakotte, E. Brück, F. R. de Boer, L. Havela, V. Sechovský, P. Svoboda, and H. Maletta, IEEE Trans. Magn. **30**, 1214 (1994).

[8] V. Sechovský, L. Havela, A. Purwanto, A. C. Larson, R. A. Robinson, K. Prokeš, H. Nakotte, E. Brück, F. R. de Boer, P. Svoboda, H. Maletta, and M. Winkelmann, J. Alloys Compd. **213/214**, 536 (1994).

[9] V. Sechovský, L. Havela, P. Svoboda, A. Purwanto, A. C. Larson, R. A. Robinson, K. Prokeš, H. Nakotte, F. R. de Boer, and H. Maletta, J. Appl. Phys. **76**, 6217 (1994).

[10] A. Purwanto, V. Sechovský, L. Havela, R. A. Robinson, H. Nakotte, A. C. Larson, K. Prokeš, E. Brück, and F. R. de Boer, Phys. Rev. B **53**, 758 (1996).

[11] F. R. de Boer, K. Prokeš, H. Nakotte, E. Brück, M. Hilbers, P. Svoboda, V. Sechovský, L. Havela, and H. Maletta, Physica B **201**, 251 (1994).

[12] A. C. Larson and R. B. Von Dreele (unpublished).

[13] G. L. Squires, *Introduction to the Theory of Thermal Neutron Scattering* (Cambridge University Press, Cambridge, 1978), p. 177.

[14] L. M. Sandratskii and J. Kübler, Phys. Rev. Lett. **75**, 946 (1995).

[15] A. Purwanto, Ph.D. thesis, New Mexico State University, Las Cruces, 1995.